Reconfigurable all-dielectric metalens based on phase change materials

Reconfigurable all-dielectric metalens for diffraction-limited imaging

Shalaginov, Mikhail, An, Sensong, Zhang, Yifei, Yang, Fan, Su, Peter, et al.

Mikhail Y. Shalaginov, Sensong An, Yifei Zhang, Fan Yang, Peter Su, Vladimir Liberman, Jeffrey B. Chou, Christopher M. Roberts, Myungkoo Kang, Carlos Rios, Qingyang Du, Clayton Fowler, Anuradha Agarwal, Kathleen A. Richardson, Clara Rivero-Baleine, Hualiang Zhang, Juejun Hu, Tian Gu, "Reconfigurable all-dielectric metalens for diffraction-limited imaging," Proc. SPIE 11461, Active Photonic Platforms XII, 114610M (20 August 2020); doi: 10.1117/12.2565267

SPIE.

Event: SPIE Nanoscience + Engineering, 2020, Online Only

Reconfigurable all-dielectric metalens for diffraction-limited imaging

Mikhail Y. Shalaginov[a], Sensong An[b], Yifei Zhang[a], Fan Yang[a], Peter Su[a], Vladimir Liberman[c], Jeffrey B. Chou[c], Christopher M. Roberts[c], Myungkoo Kang[d], Carlos Rios[a], Qingyang Du[a], Clayton Fowler[b], Anuradha Agarwal[a], Kathleen A. Richardson[d], Clara Rivero-Baleine[e], Hualiang Zhang[b], Juejun Hu[a], and Tian Gu*[a]

[a]Department of Materials Science and Engineering, Massachusetts Institute of Technology, Cambridge, Massachusetts 02139, USA; [b]Department of Electrical & Computer Engineering, University of Massachusetts Lowell, Lowell, MA, USA; [c]Lincoln Laboratory, Massachusetts Institute of Technology, Lexington, MA, USA; [d]The College of Optics & Photonics, Department of Materials Science and Engineering, University of Central Florida, Orlando, FL, USA; [e]Missiles and Fire Control, Lockheed Martin Corporation, Orlando, FL, USA

ABSTRACT

Optical metasurfaces, planar sub-wavelength nano-antenna arrays with the singular ability to sculpt wave front in almost arbitrary manners, are poised to become a powerful tool enabling compact and high-performance optics with novel functionalities. A particularly intriguing research direction within this field is active metasurfaces, whose optical response can be dynamically tuned post-fabrication, thus allowing a plurality of applications unattainable with traditional bulk optics. The efforts to date, however, still face major performance limitations in tuning range, optical quality, and efficiency especially for non-mechanical actuation mechanisms. In this paper, we introduce an active metasurface platform combining phase tuning covering the full 2π range and diffraction-limited performance using an all-dielectric, low-loss architecture based on optical phase change materials (O-PCMs). We present a generic design principle enabling binary switching of metasurfaces between arbitrary phase profiles. We implement the approach to realize a high-performance varifocal metalens. The metalens is constructed using $Ge_2Sb_2Se_4Te_1$ (GSST), an O-PCM with a large refractive index contrast and unique broadband low-loss characteristics in both amorphous and crystalline states. The reconfigurable metalens features focusing efficiencies above 20% at both states for linearly polarized light and a record large switching contrast ratio (*CR*) close to 30 dB. We further validate aberration-free and multi-depth imaging using the metalens, which represents the first experimental demonstration of a non-mechanical active metalens with diffraction-limited performance.

Keywords: active metasurface, phase change materials, metalens

1. INTRODUCTION

Optical metasurfaces consist of nano-structured meta-atoms arranged in subwavelength arrays that allow on-demand manipulation of the phase, amplitude, and polarization of light[1–8]. The promise of metasurface optics lies in the arbitrary control of electromagnetic waves with an optically-thin form factor that cannot be obtained by traditional bulk optics. Integrated with active components, the flat, pixelated metasurface architecture further facilitates the local and global tuning of their optical responses. These tunable devices are customarily known as active metasurfaces.

Active metasurfaces have received concentrated attention recently, emerging as a promising area on the path towards practical implementations[9–16]. Mechanical deformation or displacement of metasurfaces is an effective method for tuning metasurface devices or adaptively correcting optical aberrations[17–22]. On the other hand, non-mechanical actuation methods, which allow direct modulation of optical properties of meta-atoms, can offer significant advantages in terms of speed, power consumption, reliability, as well as design flexibility. A variety of tuning mechanisms such as free carrier[23], thermo-optic[24], electro-refractive[25], and all-optical[26] effects have been harnessed to create active metasurface devices. However, these effects are either relatively weak (e.g., thermo-optic, electro-refractive, and all-optical effects) or incur excessive optical loss (e.g., free carrier injection). Consequently, the tuning range and optical efficiency of these active metasurfaces are often limited.

*gutian@mit.edu

Active Photonic Platforms XII, edited by Ganapathi S. Subramania, Stavroula Foteinopoulou, Proc. of SPIE Vol. 11461, 114610M · © 2020 SPIE · CCC code: 0277-786X/20/$21 · doi: 10.1117/12.2565267

Phase change and phase transition materials (exemplified by chalcogenide compounds and correlated oxides such as VO_2, respectively) offer another promising route for realizing active metasurfaces[16,27–29]. The extremely large refractive index contrast associated with material phase transformation (e.g. $\Delta n > 1$) uniquely empowers metasurface devices with ultra-wide tuning ranges. Many studies have achieved amplitude or spectral tailoring of light via metastructures made of these materials[30–39]. Tunable optical phase or wavefront control, which is essential for realizing multifunctional meta-optical components, such as, metalenses and beam steering devices, has also been demonstrated[40–43]. However, that meta-optical devices had relatively low efficiencies, and their phase precision, a key metric which dictates optical quality of metasurface devices, has not been quantified. Moreover, the designs often suffer from significant crosstalk between the optical states which causes ghosting across the variable states and severe image quality degradation in imaging applications. As a result, it is not clear yet whether active meta-optical devices can possibly attain diffraction-limited, low-crosstalk performances rivaling their traditional bulky refractive counterparts.

In this paper, we present a generic design methodology enabling switching of metasurface devices to realize arbitrary phase profiles. The concept of a varifocal lens based on phase change materials was first elegantly implemented in the pioneering work by Yin *et al.*[43]. Their design relied on two groups of plasmonic antennae sharing the same lens aperture on top of a blanket phase change material film, each of which responded to incident light at either the amorphous or crystalline state of the film. The shared-aperture layout and the use of metallic meta-atoms limited the focusing efficiencies to 5% and 10% in the two states. Our device instead builds on all-dielectric meta-atom structures optimized via design methodology to simultaneously minimize phase error (thereby suppressing crosstalk) and boost optical efficiency. We have further experimentally demonstrated diffraction-limited imaging free of aberration and crosstalk at both states of the metalens, for the first time proving that active metasurface optics based on O-PCM technologies can indeed attain a high level of optical quality matching that of their conventional bulk counterparts while taking full advantage of their flat optical architecture.

2. ON-DEMAND COMPOSITION OF BI-STATE META-OPTICAL DEVICES

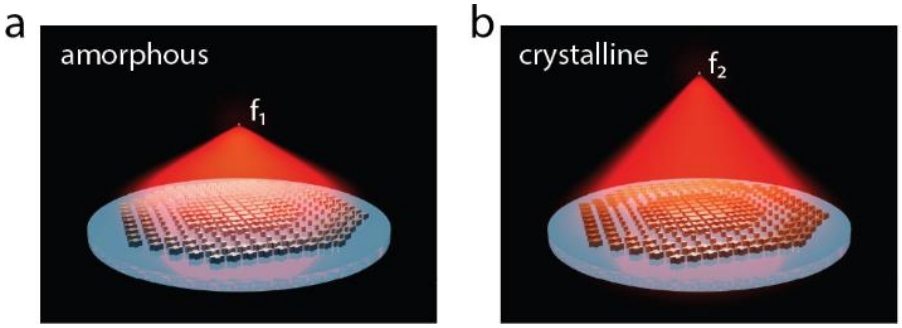

Figure 1. Artistic rendering of a reconfigurable varifocal metalens[44]

We select $Ge_2Sb_2Se_4Te_1$ (GSST) as the O-PCM to construct the metasurface operating at the wavelength $\lambda_0 = 5.2$ μm. Compared to the classical $Ge_2Sb_2Te_5$ (GST) phase change alloy, GSST offers exceptionally broadband transparency in the infrared spectral regime for both its amorphous and crystalline phases, a feature critical to optical loss reduction, while maintaining a large refractive index contrast between the two states[45–48]. The metasurface consists of patterned, isolated GSST Huygens meta-atoms sitting on a CaF_2 substrate (Fig. 1). The Huygens-type meta-atom design features an ultra-thin, deep sub-wavelength profile ($< \lambda_0/5$) which facilitates a simple one-step etch fabrication process[49–52]. While here we use a bi-state varifocal metalens as our proof-of-concept demonstration, our device architecture and design approach are generic and applicable to active metasurfaces switchable between arbitrary phase profiles. The design can also be readily generalized to active metasurfaces supporting more than two optical states, for instance leveraging intermediate states in O-PCMs[53–55].

The design procedure of the active metalens with a dimension of 1.5×1.5 mm^2 is illustrated in Fig. 2. The design process starts by defining the target phase maps in the two optical states. For the varifocal metalens under consideration, two hyperbolic phase profiles (with 2π phase wraps) yielding focal lengths of $f_1 = 1.5$ mm (amorphous, a-state) and $f_2 = 2$ mm (crystalline, c-state) are plotted in Figs. 2a and 2f, respectively. The design corresponds to numerical aperture (NA) values of 0.45 and 0.35 in the amorphous and crystalline states, respectively. We then choose to discretize the continuous 0 to 2π phase profiles into $m = 4$ phase levels, i.e., 0, $\pi/2$, π, and $3\pi/2$ (Figs. 2b and 2g). To enable switching

between two arbitrary phase profiles with four discrete phase levels, a total of $m^2 = 16$ meta-atom designs are needed, each of which provides a distinct combination of two of the four discrete phase values during the phase transition. An ideal meta-atom design must minimize phase error while maximizing optical efficiency at both states.

To obtain the 16 optimal meta-atom designs, a pool of Huygens meta-atoms with various regular geometries, such as 'I', 'H', and "+" shapes, were first generated by sweeping the geometric parameters in a full-wave electromagnetic solver, and then grouped according to the four phase levels and phase variances between the two states. Different sub-groups of meta-atoms were then mapped onto the evenly-discretized metasurface phase profiles.

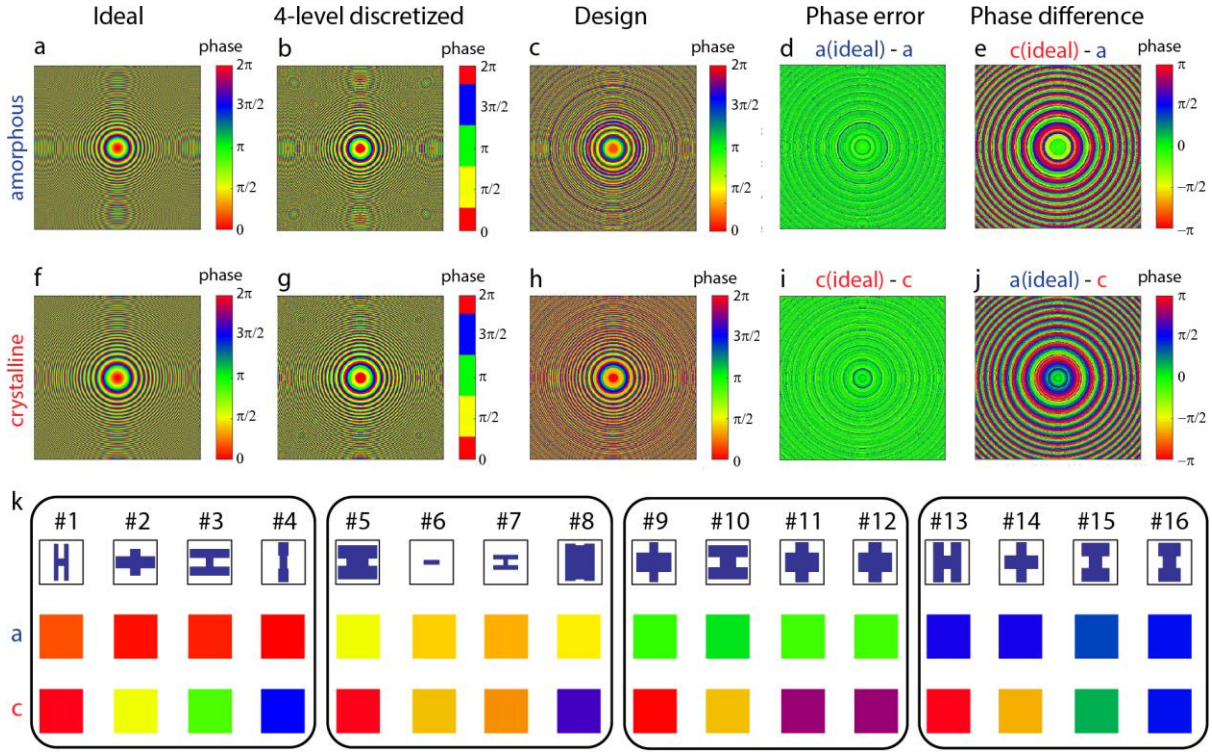

Figure 2. 2-D phase maps of the metalens in (a-c) amorphous and (f-h) crystalline states: (a, f) ideal target phase profiles with continuous phase distribution; (b, g) 4-level discretized phase profiles; and (c, h) final design taking into account phase responses of the meta-atoms. (d, e, i, j) Difference between the ideal and final design phase maps at the (d, i) primary and (e, j) phantom focal planes. (k) 16 meta-atoms selected to construct the reconfigurable metalens. Different colors correspond to the phase values shown in (c, h) [44].

3. METALENS FABRICATION AND CHARACTERIZATION

The metalens was patterned in thermally evaporated GSST films on a CaF_2 substrate using electron beam lithography (EBL) and standard plasma etching. GSST films of nominally 1 μm thickness were deposited onto a double-side polished CaF_2 (111) substrate (MTI Corp.) by thermal co-evaporation in a custom-made system (PVD Products Inc.)[56]. The desired film stoichiometry was achieved by controlling the ratio of evaporation rates of two isolated targets of $Ge_2Sb_2Te_5$ and $Ge_2Sb_2Se_5$. The deposition rates were kept at 4.3 Å/s ($Ge_2Sb_2Te_5$) and 12 Å/s ($Ge_2Sb_2Se_5$) with a base pressure of 2.8×10^{-6} Torr and a sample holder rotation speed of 6 rpm. The substrate was held near room temperature throughout the film deposition process. Thickness of the film was measured with a stylus profilometer (Bruker DXT) to be 1.10 μm (a-state) and 1.07 μm (c-state), indicating 3% volumetric contraction during crystallization similar to other phase change materials[57,58]. The film was patterned via EBL on an Elionix ELS-F125 system followed by reactive ion etching (Plasmatherm, Shuttlelock System VII SLR-770/734). The electron beam writing was carried out on an 800-nm-thick layer of ZEP520A resist, which was spin coated on top of the GSST film at 2,000 rpm for 1 min and then baked at 180°C for 1 min. Before resist coating, the sample surface was treated with standard oxygen plasma cleaning to improve resist adhesion. To prevent charging effects during the electron beam writing process, the photoresist was covered with a water-soluble conductive polymer (ESpacer 300Z, Showa Denko America, Inc.)[59]. The EBL writing was performed with

a voltage of 125 kV, 120 μm aperture, and 10 nA writing current. Proximity error correction was also implemented with a base dose time of 0.03 μs/dot (which corresponds to a dosage of 300 μC/cm^2). The exposed photoresist was developed by subsequently immersing the sample into water, ZED-N50 (ZEP developer), methyl isobutyl ketone (MIBK), and isopropanol alcohol (IPA) for 1 min each. Reactive ion etching was performed with a gas mixture of CHF_3:CF_4 (3:1) with respective flow rates of 45 sccm and 15 sccm, pressure of 10 mTorr, and RF power of 200 W. The etching rate was approximately 80 nm/min. The etching was done in three cycles of 5 mins with cooldown breaks of several minutes in between. After completing the etching step, the sample was soaked in N-methyl-2-pyrrolidone (NMP) overnight to remove the residual ZEP resist mask. After optical characterization of the metalens in the amorphous (as-deposited) state, the sample was transitioned to the crystalline state by hot-plate annealing at 250°C for 30 minutes. The annealing was conducted in a glovebox filled with an ultra high purity argon atmosphere. Figure 3 presents scanning electron microscopy (SEM) images of the fabricated metasurfaces. The meta-atoms show negligible surface roughness, almost vertical sidewalls with a sidewall angle > 85°, and excellent pattern fidelity consistent with our design.

The metalens was characterized using an external cavity tunable quantum cascade laser (QCL) emitting linearly polarized light at 5.2 μm wavelength. The collimated laser beam was focused by the metalens and images of the focal spots were first magnified with a double-lens microscope assembly (with a calibrated magnification of 120) and then recorded by a liquid nitrogen cooled InSb focal plane array (FPA) camera on the two focal planes (f_1 = 1.5 mm and f_2 = 2 mm). The focal spot images are shown in Fig. 4 insets and the main panels in Fig. 4 plot the optical intensity profiles across the center planes of the focal spots along with those of ideal aberration-free lenses of the same NAs. The metalens features high Strehl ratios of > 0.99 and 0.97 in the amorphous and crystalline states, respectively, implying that the lens operates in the diffraction-limited regime at both states. We further experimentally measured the focused power ratios between the true and phantom focal spots, yielding $P_{1,a}$ / $P_{2,a}$ = 10 and $P_{2,c}$ / $P_{1,c}$ = 90. The result corresponds to a large *CR* of 29.5 dB, the highest reported value to date in active metasurface devices.

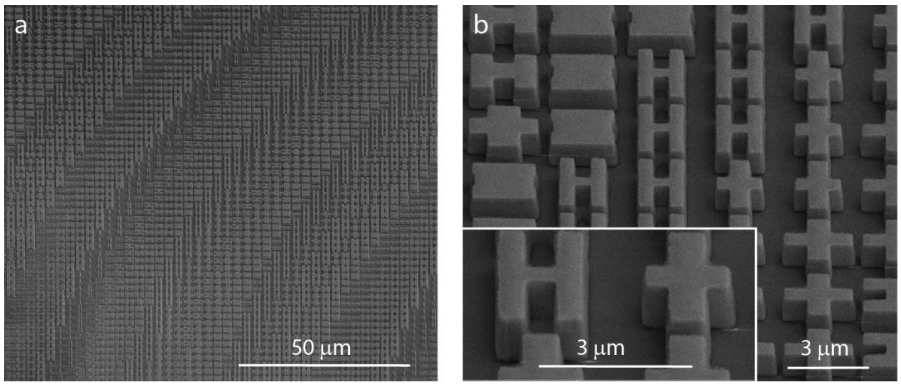

Figure 3. SEM images of the metalens showing the GSST meta-atoms with vertical sidewalls and excellent pattern fidelity.

Focusing efficiency of the metalens was quantified following our previously established measurement protocols[60]. Focusing efficiencies of 23.7% and 21.6% were measured for the amorphous and crystalline states, respectively. The difference between the experimental results and theoretical predictions are primarily due to meta-atom geometry and refractive index deviations in the fabricated device. However, the demonstrated performance still represents major improvements over prior state-of-the-art in varifocal metalens.

Finally, we demonstrated high-resolution, low-crosstalk imaging using our reconfigurable metalens. Standard USAF 1951 resolution charts in the form of Sn patterns fabricated on CaF_2 discs were used as the imaging objects. The imaging object comprises one or two resolution charts coinciding with the two focal planes (f_1 = 1.5 mm and f_2 = 2 mm) which are flood-illuminated from the backside using the QCL. The metalens was used as an objective to project the resolution target images onto the camera. Figure 5a shows four images of the resolution charts captured using the setup when only a single resolution target was placed at one of the focal planes. The lens produced clearly resolved images of the USAF 6.2 (half-period 7 μm) and USAF 5.6 (half period 8.8 μm) patterns when the lens was in amorphous and crystalline states, respectively. This result agrees well with theoretical resolution limits of 7 μm and 9 μm in the two states, suggesting that our metalens can indeed achieve diffraction-limited imaging performance. In contrast, no image was observed when the resolution target was placed at the phantom focal plane.

We further show that the metalens can be used for imaging multi-depth objects with minimal crosstalk. In the test, two resolution targets were each positioned at one focal plane with 45° relative in-plane rotation with respect to the other target. At each optical state of the metalens, only one resolution target aligning with the focal plane was clearly imaged with no sign of ghost image resulting from the other target (Fig. 5b). These results prove that the active metalens is capable of diffraction-limited imaging free of optical aberrations and crosstalk across overlapping objects at different depths.

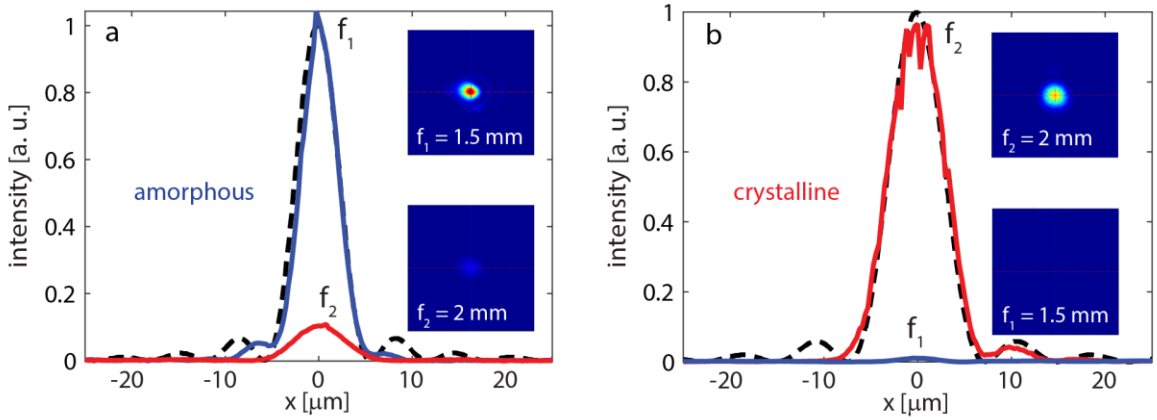

Figure 4. Optical characterization. Focal spot profiles for the metalens in two states: (a) amorphous and (b) crystalline. Each plot contains the focal spot intensity distributions for the f_1 = 1.5 mm and f_2 = 2 mm focal planes. All the focal spots are diffraction-limited. The focal spots produced by ideal, aberration-free lenses of the same NA are marked with black dashed-curves. The insets show the 2-D images of the focal spots: f_1 = 1.5 mm and f_2 = 2mm. Power contrast ratios are 10:1 and 90:1 for the a- and c-states, respectively.

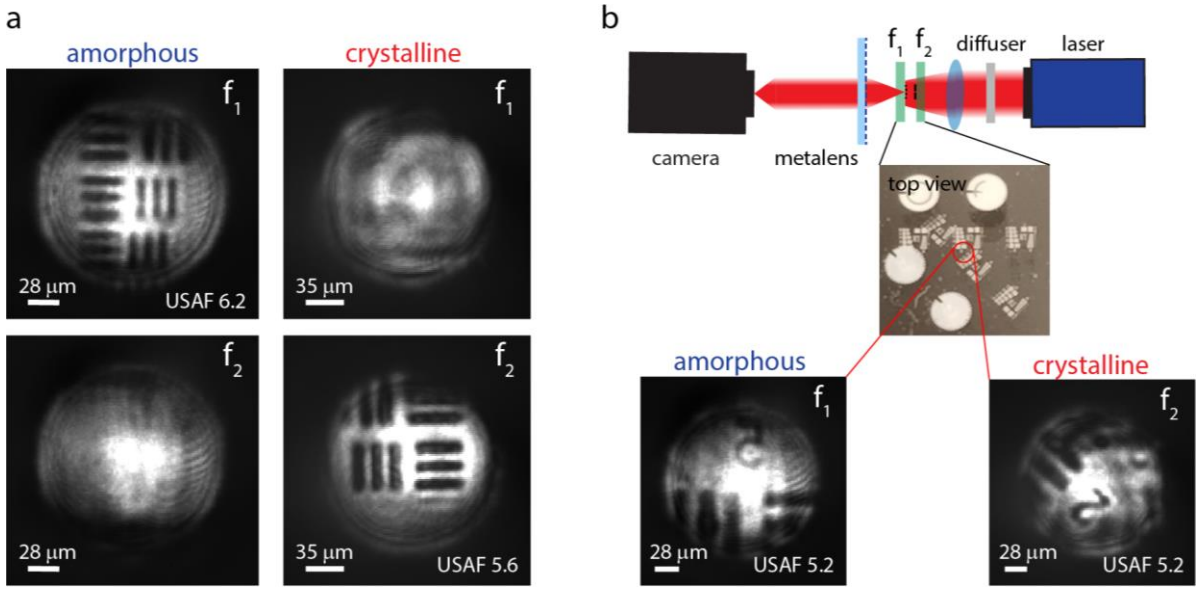

Figure 5. Imaging using the GSST varifocal metalens. (a) Well-resolved lines of USAF resolution charts: the patterns have half periods close to the Rayleigh resolution limits of 7 μm and 9 μm in the a-state (f_1) and c-state (f_2), respectively. (b) Schematic of the setup for imaging multi-depth targets. Top-view photograph of the target consisting of two patterned samples overlapped at an angle of 45°. Camera images of the dual-depth target acquired by a stationary metalens in a- and c-states.

4. DISCUSSION

Our work demonstrates that judiciously engineered active metasurfaces can achieve high optical quality in the diffraction-limited regime rivaling the performance of traditional aspheric refractive optics. The high-performance meta-optics as well as the efficient design approach will open up many exciting applications involving reconfigurable or adaptive optics. For instance, the varifocal metalens constitutes a key building block for a parfocal lens (a true zoom lens which stays in focus while changing magnification) widely used in cameras, microscopes, telescopes, and video recorders. Conventional parfocal zoom lenses necessarily involve multiple mechanically moving elements required for aberration compensation while tuning the magnification, which severely compromise the size, complexity, ruggedness, and often image quality. In contrast, our varifocal metalens enables a drastically simplified step-zoom parfocal lens design consisting of only two phase-change metasurfaces patterned on the top and bottom surfaces of a single flat substrate, while maintaining diffraction-limited imaging performance. Besides imaging, the active metasurface can potentially also enable other applications such as beam steering, adaptive optics, and optical spectroscopy[61].

Switching from the amorphous to the crystalline phase was accomplished via furnace annealing in our present prototype. Practical deployment of the active, reversible reconfigurable metasurface will necessarily involve electrical switching of O-PCMs. We have recently demonstrated highly consistent electrothermal switching of GSST over 1,000 phase transition cycles using on-chip metal micro-heaters[45]. Additionally, reversible switching of GSST and other phase change materials using transparent graphene and doped Si heaters have also been validated[62–64]. In this regard, the use of GSST rather than the classical GST alloy uniquely benefits from not only GSST's low optical attenuation but also its improved amorphous phase stability. GST boasts a short crystallization time in the nanosecond regime[65], which is useful for ultrafast switching but at the same time also limits the critical thickness amenable to fully reversible switching to less than 100 nm. In comparison, while the detailed crystallization kinetics of GSST has not yet been quantified[66], its crystallization time is likely in the order of microseconds. This much longer crystallization time permits reversible switching of GSST films with thicknesses exceeding 1 μm, presenting a critical benefit for their photonic applications. Indeed, we have recently reported what we believe to be the first electrically reconfigurable metasurface based on O-PCMs at the 1550 nm telecommunication band, where the entire meta-atoms (250 nm in thickness) are made of GSST. The ensuing large optical modal overlap with the active O-PCM enables spectral tuning of resonances across a record broad half-octave band[67]. These advances define a clear path towards practical implementation of the active metasurface design with integrated transparent heaters.

Finally, even though our metalens already claims exceptional optical quality, our generic design principle points to several future improvements which can further enhance lens performance and design versatility. Our present metalens uses four discrete phase levels, which imposes ~ 20% efficiency loss due to discretization phase errors[68]. The conventional searching method based on parameter sweeping limits the size of the accessible unit cell library in practice. Increasing the number of phase discretization levels m contributes to mitigating phase errors and increasing focusing efficiency. One can also scale the design approach to three or more arbitrary optical states taking advantage of intermediate states and the large index contrast afforded by O-PCMs[53,54]. In general, an active metasurface with j optical states ($j \geq 2$) each characterized by m phase levels demands a minimum of m^j distinct meta-atoms. The design problem, whose complexity escalates rapidly with increasing m and j, is best handled with deep learning based meta-atom design algorithms[69,70] and will be the subject of a follow-up paper.

5. CONCLUSION

In conclusion, we propose a non-mechanical active metasurface design to realize binary or multi-configuration switching between arbitrary optical states. We validated the design principle by fabricating a varifocal metalens using low-loss O-PCM GSST, and demonstrated aberration and crosstalk-free imaging. The work proves that non-mechanical active metasurfaces can achieve optical quality on par with conventional precision bulk optics involving mechanical moving parts, thereby pointing to a cohort of exciting applications fully unleashing the SWaP-C benefits of active metasurface optics in imaging, sensing, display, and optical ranging.

6. ACKNOWLEDGEMENTS

This work was funded by Defense Advanced Research Projects Agency Defense Sciences Office (DSO) Program: EXTREME Optics and Imaging (EXTREME) under Agreement No. HR00111720029. The authors also acknowledge characterization facility support provided by the Materials Research Laboratory at Massachusetts Institute of Technology

(MIT), as well as fabrication facility support by the Microsystems Technology Laboratories at MIT and Harvard University Center for Nanoscale Systems. The views, opinions and/or findings expressed are those of the authors and should not be interpreted as representing the official views or policies of the Department of Defense or the U.S. Government.

REFERENCES

[1] Yu, N., Genevet, P., Kats, M.A., Aieta, F., Tetienne, J.-P.J.-P., Capasso, F., Gaburro, Z., Aieta, F., Kats, M.A., et al., "Light Propagation with Phase Discontinuities: Generalized Laws of Reflection and Refraction," Science (New York, N.Y.) 334(6054), 333–337 (2011).

[2] Yu, N., and Capasso, F., "Flat optics with designer metasurfaces," Nature Materials 13(2), 139–150 (2014).

[3] Kildishev, A. V., Boltasseva, A., and Shalaev, V.M., "Planar photonics with metasurfaces," in Science (80-.). 339(6125), American Association for the Advancement of Science, pp. 12320091–12320096 (2013).

[4] Kamali, S.M., Arbabi, E., Arbabi, A., and Faraon, A., "A review of dielectric optical metasurfaces for wavefront control," Nanophotonics 7(6), 1041–1068 (2018).

[5] Lalanne, P., and Chavel, P., "Metalenses at visible wavelengths: past, present, perspectives," Laser & Photonics Reviews 11(3), 1600295 (2017).

[6] Glybovski, S.B., Tretyakov, S.A., Belov, P.A., Kivshar, Y.S., and Simovski, C.R., "Metasurfaces: From microwaves to visible," Physics Reports 634, 1–72 (2016).

[7] Neshev, D., and Aharonovich, I., "Optical metasurfaces: new generation building blocks for multi-functional optics," Light: Science & Applications 7(1), 58 (2018).

[8] Hsiao, H.-H., Chu, C.H., and Tsai, D.P., "Fundamentals and Applications of Metasurfaces," Small Methods 1(4), 1600064 (2017).

[9] Kang, L., Jenkins, R.P., and Werner, D.H., "Recent Progress in Active Optical Metasurfaces," Advanced Optical Materials 7(14), 1801813 (2019).

[10] Nemati, A., Wang, Q., Hong, M., and Teng, J., "Tunable and reconfigurable metasurfaces and metadevices," Opto-Electronic Advances 1(5), 18000901–18000925 (2018).

[11] Chen, H.-T., Taylor, A.J., and Yu, N., "A review of metasurfaces: physics and applications," Reports on Progress in Physics 79(7), 076401 (2016).

[12] Hail, C.U., Michel, A.U., Poulikakos, D., and Eghlidi, H., "Optical Metasurfaces: Evolving from Passive to Adaptive," Advanced Optical Materials 7(14), 1801786 (2019).

[13] Shaltout, A.M., Kildishev, A. V., and Shalaev, V.M., "Evolution of photonic metasurfaces: from static to dynamic," Journal of the Optical Society of America B 33(3), 501 (2016).

[14] He, Q., Sun, S., and Zhou, L., "Tunable/Reconfigurable Metasurfaces: Physics and Applications," Research 2019, 1–16 (2019).

[15] Paniagua-Dominguez, R., Ha, S.T., and Kuznetsov, A.I., "Active and Tunable Nanophotonics with Dielectric Nanoantennas," Proceedings of the IEEE 108(5), 749–771 (2020).

[16] Abdollahramezani, S., Hemmatyar, O., Taghinejad, H., Krasnok, A., Kiarashinejad, Y., Zandehshahvar, M., Alu, A., and Adibi, A., "Tunable nanophotonics enabled by chalcogenide phase-change materials," arXiv:2001.06335 (2020).

[17] Kamali, S.M., Arbabi, E., Arbabi, A., Horie, Y., and Faraon, A., "Highly tunable elastic dielectric metasurface lenses," Laser & Photonics Reviews 10(6), 1002–1008 (2016).

[18] Ee, H.-S., and Agarwal, R., "Tunable Metasurface and Flat Optical Zoom Lens on a Stretchable Substrate," Nano Letters 16(4), 2818–2823 (2016).

[19] She, A., Zhang, S., Shian, S., Clarke, D.R., and Capasso, F., "Adaptive metalenses with simultaneous electrical control of focal length, astigmatism, and shift," Science Advances 4(2), 1–8 (2018).

[20] Zhu, L., Kapraun, J., Ferrara, J., and Chang-Hasnain, C.J., "Flexible photonic metastructures for tunable coloration," Optica 2(3), 255 (2015).

[21] Arbabi, E., Arbabi, A., Kamali, S.M., Horie, Y., Faraji-Dana, M., and Faraon, A., "MEMS-tunable dielectric metasurface lens," Nature Communications 9(1), 812 (2018).

[22] Roy, T., Zhang, S., Jung, I.W., Troccoli, M., Capasso, F., and Lopez, D., "Dynamic metasurface lens based on MEMS technology," APL Photonics 3(2), 021302 (2018).

[23] Morea, M., Zang, K., Kamins, T.I., Brongersma, M.L., and Harris, J.S., "Electrically Tunable, CMOS-

Compatible Metamaterial Based on Semiconductor Nanopillars," ACS Photonics 5(11), 4702–4709 (2018).
[24] Rahmani, M., Xu, L., Miroshnichenko, A.E., Komar, A., Camacho-Morales, R., Chen, H., Zárate, Y., Kruk, S., Zhang, G., et al., "Reversible Thermal Tuning of All-Dielectric Metasurfaces," Advanced Functional Materials 27(31), 1700580 (2017).
[25] Decker, M., Kremers, C., Minovich, A., Staude, I., Miroshnichenko, A.E., Chigrin, D., Neshev, D.N., Jagadish, C., and Kivshar, Y.S., "Electro-optical switching by liquid-crystal controlled metasurfaces," Optics Express 21(7), 8879 (2013).
[26] Shcherbakov, M.R., Liu, S., Zubyuk, V. V., Vaskin, A., Vabishchevich, P.P., Keeler, G., Pertsch, T., Dolgova, T. V., Staude, I., et al., "Ultrafast all-optical tuning of direct-gap semiconductor metasurfaces," Nature Communications 8(1), 17 (2017).
[27] Wuttig, M., Bhaskaran, H., and Taubner, T., "Phase-change materials for non-volatile photonic applications," Nature Photonics 11(8), 465–476 (2017).
[28] Zhang, W., Mazzarello, R., and Ma, E., "Phase-change materials in electronics and photonics," MRS Bulletin 44(09), 686–690 (2019).
[29] Ding, F., Yang, Y., and Bozhevolnyi, S.I., "Dynamic Metasurfaces Using Phase-Change Chalcogenides," Advanced Optical Materials 7(14), 1801709 (2019).
[30] Dicken, M.J., Aydin, K., Pryce, I.M., Sweatlock, L.A., Boyd, E.M., Walavalkar, S., Ma, J., and Atwater, H.A., "Frequency tunable near-infrared metamaterials based on VO2 phase transition," Optics Express 17(20), 18330 (2009).
[31] Zhu, Z., Evans, P.G., Haglund, R.F., and Valentine, J.G., "Dynamically Reconfigurable Metadevice Employing Nanostructured Phase-Change Materials," Nano Letters 17(8), 4881–4885 (2017).
[32] Kats, M.A., Blanchard, R., Genevet, P., Yang, Z., Qazilbash, M.M., Basov, D.N., Ramanathan, S., and Capasso, F., "Thermal tuning of mid-infrared plasmonic antenna arrays using a phase change material," Optics Letters 38(3), 368 (2013).
[33] Carrillo, S.G., Trimby, L., Au, Y., Nagareddy, V.K., Rodriguez-Hernandez, G., Hosseini, P., Ríos, C., Bhaskaran, H., and Wright, C.D., "A Nonvolatile Phase-Change Metamaterial Color Display," Advanced Optical Materials 7(18), 1801782 (2019).
[34] Tittl, A., Michel, A.U., Schäferling, M., Yin, X., Gholipour, B., Cui, L., Wuttig, M., Taubner, T., Neubrech, F., et al., "A Switchable Mid-Infrared Plasmonic Perfect Absorber with Multispectral Thermal Imaging Capability," Advanced Materials 27, 4597–4603 (2015).
[35] Cao, T., Zhang, X., Dong, W., Lu, L., Zhou, X., Zhuang, X., Deng, J., Cheng, X., Li, G., et al., "Tuneable Thermal Emission Using Chalcogenide Metasurface," Advanced Optical Materials 6(16), 1800169 (2018).
[36] Du, K.-K., Li, Q., Lyu, Y.-B., Ding, J.-C., Lu, Y., Cheng, Z.-Y., and Qiu, M., "Control over emissivity of zero-static-power thermal emitters based on phase-changing material GST," Light: Science & Applications 6(1), e16194–e16194 (2017).
[37] Du, K., Cai, L., Luo, H., Lu, Y., Tian, J., Qu, Y., Ghosh, P., Lyu, Y., Cheng, Z., et al., "Wavelength-tunable mid-infrared thermal emitters with a non-volatile phase changing material," Nanoscale 10(9), 4415–4420 (2018).
[38] Pogrebnyakov, A. V., Bossard, J.A., Turpin, J.P., Musgraves, J.D., Shin, H.J., Rivero-Baleine, C., Podraza, N., Richardson, K.A., Werner, D.H., et al., "Reconfigurable near-IR metasurface based on $Ge_2Sb_2Te_5$ phase-change material," Optical Materials Express 8(8), 2264 (2018).
[39] Dong, W., Qiu, Y., Zhou, X., Banas, A., Banas, K., Breese, M.B.H., Cao, T., and Simpson, R.E., "Tunable Mid-Infrared Phase-Change Metasurface," Advanced Optical Materials 6(14), 1701346 (2018).
[40] Dong, K., Hong, S., Deng, Y., Ma, H., Li, J., Wang, X., Yeo, J., Wang, L., Lou, S., et al., "A Lithography-Free and Field-Programmable Photonic Metacanvas," Advanced Materials 30(5), 1703878 (2018).
[41] Wang, Q., Rogers, E.T.F., Gholipour, B., Wang, C.-M., Yuan, G., Teng, J., and Zheludev, N.I., "Optically reconfigurable metasurfaces and photonic devices based on phase change materials," Nature Photonics 10(1), 60–65 (2015).
[42] de Galarreta, C.R., Alexeev, A.M., Au, Y.-Y., Lopez-Garcia, M., Klemm, M., Cryan, M., Bertolotti, J., and Wright, C.D., "Nonvolatile Reconfigurable Phase-Change Metadevices for Beam Steering in the Near Infrared," Advanced Functional Materials 28(10), 1704993 (2018).
[43] Yin, X., Steinle, T., Huang, L., Taubner, T., Wuttig, M., Zentgraf, T., and Giessen, H., "Beam switching and bifocal zoom lensing using active plasmonic metasurfaces," Light: Science & Applications 6(7), e17016 (2017).
[44] Shalaginov, M.Y., An, S., Zhang, Y., Yang, F., Su, P., Liberman, V., Chou, J.B., Roberts, C.M., Kang, M., et al., "Reconfigurable all-dielectric metalens with diffraction limited performance," arXiv:1911.12970 (2019).

[45] Zhang, Y., Chou, J.B., Li, J., Li, H., Du, Q., Yadav, A., Zhou, S., Shalaginov, M.Y., Fang, Z., et al., "Broadband transparent optical phase change materials for high-performance nonvolatile photonics," Nature Communications 10, 4279 (2019).
[46] Zhang, Q., Zhang, Y., Li, J., Soref, R., Gu, T., and Hu, J., "Broadband nonvolatile photonic switching based on optical phase change materials: beyond the classical figure-of-merit," Optics Letters 43(1), 94 (2018).
[47] Zhang, Y., Li, J., Chou, J., Fang, Z., Yadav, A., Lin, H., Du, Q., Michon, J., Han, Z., et al., "Broadband Transparent Optical Phase Change Materials," Conference on Lasers and Electro-Optics(c), JTh5C.4 (2017).
[48] Zhang, Y., and Hu, J., "Reconfigurable optics-a phase change for the better," AMERICAN CERAMIC SOCIETY BULLETIN 99(4), 36–37 (2020).
[49] Decker, M., Staude, I., Falkner, M., Dominguez, J., Neshev, D.N., Brener, I., Pertsch, T., and Kivshar, Y.S., "High-Efficiency Dielectric Huygens' Surfaces," Advanced Optical Materials 3(6), 813–820 (2015).
[50] Chen, M., Kim, M., Wong, A.M.H., and Eleftheriades, G. V., "Huygens' metasurfaces from microwaves to optics: A review," Nanophotonics 7(6), 1207–1231 (2018).
[51] Shalaev, M.I., Sun, J., Tsukernik, A., Pandey, A., Nikolskiy, K., and Litchinitser, N.M., "High-Efficiency All-Dielectric Metasurfaces for Ultracompact Beam Manipulation in Transmission Mode," Nano Letters 15(9), 6261–6266 (2015).
[52] Zhang, L., Ding, J., Zheng, H., An, S., Lin, H., Zheng, B., Du, Q., Yin, G., Michon, J., et al., "Ultra-thin high-efficiency mid-infrared transmissive Huygens meta-optics," Nature Communications 9(1), 1481 (2018).
[53] Li, X., Youngblood, N., Ríos, C., Cheng, Z., Wright, C.D., Pernice, W.H., and Bhaskaran, H., "Fast and reliable storage using a 5 bit, nonvolatile photonic memory cell," Optica 6(1), 1 (2019).
[54] Rios, C., Stegmaier, M., Cheng, Z., Youngblood, N., Wright, C.D., Pernice, W.H.P., and Bhaskaran, H., "Controlled switching of phase-change materials by evanescent-field coupling in integrated photonics [Invited]," Optical Materials Express 8(9), 2455 (2018).
[55] Ríos, C., Zhang, Y., Shalaginov, M., Deckoff-Jones, S., Wang, H., An, S., Zhang, H., Kang, M., Richardson, K.A., et al., "Multi-level Electro-thermal Switching of Optical Phase-Change Materials Using Graphene," arXiv:2007.07944 (2020).
[56] Hu, J., Tarasov, V., Agarwal, A., Kimerling, L., Carlie, N., Petit, L., and Richardson, K., "Fabrication and testing of planar chalcogenide waveguide integrated microfluidic sensor," Optics Express 15(5), 2307 (2007).
[57] Nazeer, H., Bhaskaran, H., Woldering, L.A., and Abelmann, L., "Young's modulus and residual stress of GeSbTe phase-change thin films," Thin Solid Films 592, 69–75 (2015).
[58] Leervad Pedersen, T.P., Kalb, J., Njoroge, W.K., Wamwangi, D., Wuttig, M., and Spaepen, F., "Mechanical stresses upon crystallization in phase change materials," Applied Physics Letters 79(22), 3597–3599 (2001).
[59] Lin, H., Li, L., Deng, F., Ni, C., Danto, S., Musgraves, J.D., Richardson, K., and Hu, J., "Demonstration of mid-infrared waveguide photonic crystal cavities," Optics Letters 38(15), 2779–2782 (2013).
[60] Shalaginov, M.Y., An, S., Yang, F., Su, P., Lyzwa, D., Agarwal, A., Zhang, H., Hu, J., and Gu, T., "A single-layer panoramic metalens with > 170 degree diffraction-limited field of view," arXiv: 1908.03626 (2019).
[61] Kita, D.M., Miranda, B., Favela, D., Bono, D., Michon, J., Lin, H., Gu, T., and Hu, J., "High-performance and scalable on-chip digital Fourier transform spectroscopy," Nature Communications 9(1), 4405 (2018).
[62] Zheng, J., Fang, Z., Wu, C., Zhu, S., Xu, P., Doylend, J.K., Deshmukh, S., Pop, E., Dunham, S., et al., "Nonvolatile Electrically Reconfigurable Integrated Photonic Switch Enabled by a Silicon PIN Diode Heater," Advanced Materials 2001218, 2001218 (2020).
[63] Ríos, C., Zhang, Y., Deckoff-Jones, S., Li, H., Chou, J.B., Wang, H., Shalaginov, M., Roberts, C., Gonçalves, C., et al., "Reversible Switching of Optical Phase Change Materials Using Graphene Microheaters," in Conf. Lasers Electro-Optics, SF2H.4 (2019).
[64] Zhang, H., Zhou, L., Xu, J., Wang, N., Hu, H., Lu, L., Rahman, B.M.A., and Chen, J., "Nonvolatile waveguide transmission tuning with electrically-driven ultra-small GST phase-change material," Science Bulletin 64(11), 782–789 (2019).
[65] Zhang, W., Mazzarello, R., Wuttig, M., and Ma, E., "Designing crystallization in phase-change materials for universal memory and neuro-inspired computing," Nature Reviews Materials 4(3), 150–168 (2019).
[66] Zhang, Y., Chou, J.B., Li, J., Li, H., Du, Q., Yadav, A., Zhou, S., Shalaginov, M.Y., Fang, Z., et al., "Broadband transparent optical phase change materials for high-performance nonvolatile photonics," Nature Communications 10(1), 1–9 (2019).
[67] Zhang, Y., Liang, J., Shalaginov, M., Deckoff-Jones, S., Ríos, C., Chou, J.B., Roberts, C., An, S., Fowler, C., et al., "Electrically Reconfigurable Nonvolatile Metasurface Using Optical Phase Change Materials," in Conf.

Lasers Electro-Optics, JTh5B.3 (2019).
[68] Aieta, F., Genevet, P., Kats, M., and Capasso, F., "Aberrations of flat lenses and aplanatic metasurfaces," Optics Express 21(25), 31530 (2013).
[69] An, S., Fowler, C., Zheng, B., Shalaginov, M.Y., Tang, H., Li, H., Zhou, L., Ding, J., Agarwal, A.M., et al., "A Deep Learning Approach for Objective-Driven All-Dielectric Metasurface Design," ACS Photonics 6(12), 3196–3207 (2019).
[70] An, S., Zheng, B., Shalaginov, M.Y., Tang, H., Li, H., Zhou, L., Ding, J., Agarwal, A.M., Rivero-Baleine, C., et al., "A Freeform Dielectric Metasurface Modeling Approach Based on Deep Neural Networks," arXiv: 2001.00121 (2020).